JACS
JOURNAL OF THE AMERICAN CHEMICAL SOCIETY
Article
pubs.acs.org/JACS

The Substrate-Bound Crystal Structure of a Baeyer–Villiger Monooxygenase Exhibits a Criegee-like Conformation

Brahm J. Yachnin,[†,⊥] Tara Sprules,[#] Michelle B. McEvoy,[†] Peter C. K. Lau,[‡,§,∥] and Albert M. Berghuis*[,†,‡,⊥]

Departments of [†]Biochemistry, [‡]Microbiology & Immunology, and [§]Chemistry, McGill University, 3649 Promenade Sir William Osler, Bellini Pavilion, Room 466, Montreal, QC, Canada H3G 0B1

[∥]Biotechnology Research Institute, National Research Council of Canada, 6100 Royalmount Avenue, Montreal, QC, Canada H4P 2R2

[#]Québec/Eastern Canada High Field NMR Facility, 3420 University Street, Room 023, Montreal, QC, Canada H3A 2A7

[⊥]Groupes de recherche GRASP et PROTEO, Canada

Supporting Information

ABSTRACT: The Baeyer–Villiger monooxygenases (BVMOs) are a family of bacterial flavoproteins that catalyze the synthetically useful Baeyer–Villiger oxidation reaction. This involves the conversion of ketones into esters or cyclic ketones into lactones by introducing an oxygen atom adjacent to the carbonyl group. The BVMOs offer exquisite regio- and enantiospecificity while acting on a wide range of substrates. They use only NADPH and oxygen as cosubstrates, and produce only $NADP^+$ and water as byproducts, making them environmentally attractive for industrial purposes. Here, we report the first crystal structure of a BVMO, cyclohexanone monooxygenase (CHMO) from *Rhodococcus* sp. HI-31 in complex with its substrate, cyclohexanone, as well as $NADP^+$ and FAD, to 2.4 Å resolution. This structure shows a drastic rotation of the $NADP^+$ cofactor in comparison to previously reported $NADP^+$-bound structures, as the nicotinamide moiety is no longer positioned above the flavin ring. Instead, the substrate, cyclohexanone, is found at this location, in an appropriate position for the formation of the Criegee intermediate. The rotation of $NADP^+$ permits the substrate to gain access to the reactive flavin peroxyanion intermediate while preventing it from diffusing out of the active site. The structure thus reveals the conformation of the enzyme during the key catalytic step. CHMO is proposed to undergo a series of conformational changes to gradually move the substrate from the solvent, via binding in a solvent excluded pocket that dictates the enzyme's chemospecificity, to a location above the flavin–peroxide adduct where catalysis occurs.

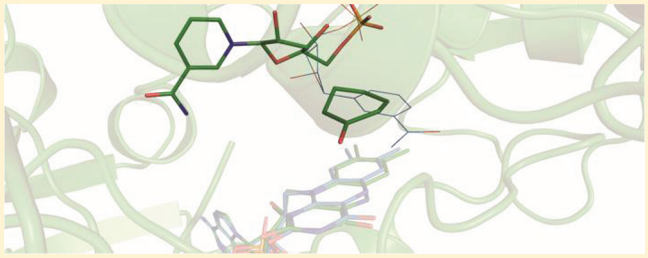

INTRODUCTION

The century-old Baeyer–Villiger (BV) reaction is the oxidative cleavage of a carbon–carbon bond adjacent to a carbonyl; this process transforms ketones to esters and cyclic ketones to lactones using peracids.[1,2] While this reaction has proven to be very useful to synthetic chemists, it has a number of shortcomings that include the use of costly and hazardous reagents or chlorinated solvents while producing more waste than product for lack of functional group selectivity and enantioselectivity. Although metal-catalyzed enantioselective BV reactions have also been developed, both cost and contamination of the products with metals may present a serious problem.[3] For a variety of reasons, Baeyer–Villiger monooxygenases (BVMOs), a family of bacterial flavoproteins that catalyze the BV reaction,[4−9] have garnered much attention. Most BVMOs are involved in the second step of biodegradation of C_5 to C_{15} alicyclic alcohols such as cyclopentanol, cyclohexanol, and cyclopentadecanol, providing a carbon source for the organisms via the formation of Krebs cycle intermediates.[6,10,11] These enzymes can function in water, and require NADPH as a cofactor and molecular oxygen as the oxidative reactant. While one oxygen atom is introduced adjacent to the carbonyl group of a ketone substrate, the other atom is reduced to water as a byproduct.[4,5,12] These green characteristics have made them intriguing targets for use as biocatalysts since the prototypical BVMO, cyclohexanone monooxygenase (CHMO) from *Acinetobacter* NCIMB 9871 (*Ac*CHMO), was first characterized nearly 40 years ago.[10,12] Their frequently exquisite regio- and enantiospecificities, combined with their broad substrate profiles that include substituted and bicyclic ketones, make them of particular interest to the pharmaceutical industry.[4−9] In recent years, a multitude of homologues of these enzymes have been cloned and characterized,[4−9] thereby expanding the range of potential substrates catalyzed by BVMOs.

Received: January 4, 2012
Published: April 16, 2012

dx.doi.org/10.1021/ja211876p | *J. Am. Chem. Soc.* 2012, 134, 7788–7795

While the BVMOs have been studied extensively, only recently has any structural data been obtained. The first BVMO to have its structure solved was phenylacetone monooxygenase (PAMO) from the thermophile *Thermobifida fisca*.[13] This structure revealed the overall fold of the enzyme and the location and conformation of the FAD prosthetic group, which remains bound throughout the catalytic cycle. Subsequently, we reported two structures of CHMO from *Rhodococcus* sp. HI-31 (*Rm*CHMO) in complex with both $NADP^+$ and FAD.[11] This enzyme is notable for being a close homologue and having a similar substrate profile to the canonical *Ac*CHMO while being substantially more stable. The two crystal structures, designated as $CHMO_{Open}$ and $CHMO_{Closed}$, revealed that $NADP^+$ can bind to the enzyme in two distinct conformations. The sliding of the $NADP^+$ cofactor deeper into the protein in the $CHMO_{Closed}$ structure was revealed to be coupled with a rotation of the NADPH-binding domain so as to create a well-defined substrate binding pocket. More recently, a series of structures of PAMO with $NADP^+$ and a weak inhibitor, 2-(*N*-morpholino)ethanesulfonic acid (MES), have corroborated these findings and provided insight into the conformation of the reduced flavoenzyme.[14] Intriguingly, the PAMO structures identified a funnel-shaped cavity that may provide an alternative entrance for the substrate to gain access to the active site. Another recent paper describing $NADP^+$-bound and $NADP^+$-free crystal structures of 2-oxo-Δ^3-4,5,5-trimethylcyclopentenyl acetyl-CoenzymeA 1,2-monooxygenase (OTEMO), which is notable for being a dimeric BVMO with a large substrate, also confirmed the dynamic nature of the BVMO family of proteins.[15] It should be noted that in addition, a crystal structure of an atypical BVMO, mithramycin monooxygenase (MtmOIV) has been obtained.[16] This enzyme has high sequence and structural similarity to a FAD-dependent hydroxylase of the glucocorticoid receptor (GR_2) subfamily. This makes it a distant relative of the prototypical BVMOs and precludes its detailed comparison with CHMO or PAMO.

Structural studies of BVMOs have provided much insight into these enzymes' catalytic mechanism; however, they have also raised questions. Notably, the $CHMO_{Closed}$ structure reveals that for the majority of CHMO's substrates, which are larger than cyclohexanone, there is actually insufficient room in the active site for the formation of the critical Criegee intermediate, the adduct of the flavin peroxide and the ketone substrate that is required for catalysis. Models of the Criegee intermediate for the cyclohexanone substrate, one of CHMO's smallest substrates, suggests that this intermediate can be achieved in the Closed conformation.[11,17] In contrast, the Criegee intermediates of larger substrates, such as substituted or bicyclic ketones on which CHMO readily acts, would result in severe steric clashes with one or more of $NADP^+$, L146, F279, and F434 in the Closed conformation. It is clear that in order for a Criegee intermediate to form, a significant reorganization of the active site is required.

Here, we present the first crystal structure of a prototypical BVMO, represented by *Rm*CHMO, bound to its substrate, cyclohexanone, as well as $NADP^+$. This structure reveals a major rotation in the $NADP^+$ cofactor, allowing CHMO to adopt a catalytically relevant conformation. The rotation permits the substrate to be positioned above the FAD, thus revealing a Criegee intermediate-like conformation, a snapshot of the most important stage of the catalytic mechanism. It also highlights the role of $NADP^+$ in organizing the active site and provides a structural explanation for the broad substrate specificity of the enzyme, which is necessary for a complete understanding of the catalytic mechanism.

EXPERIMENTAL SECTION

For a description of the subcloning of the *chnB1* gene from *Rhodococcus* sp. HI-31, the construction of various mutants for NMR and kinetic studies, and the expression and purification of the CHMO enzyme and its variants, please consult the Supporting Information.

Crystal Structure Determination. Crystals were obtained using the hanging drop vapor diffusion method. Wild-type CHMO was prepared at 5 mg/mL in 50 mM Tris pH 8.0 and supplemented with a 5× molar excess of FAD and $NADP^+$. In brief, 2 μL of protein solution was mixed with 2 μL of reservoir solution on an 18 mm siliconized coverslip (Hampton Research). The reservoir solution consisted of 0.1 M imidazole, pH 8.0, 0.2% TMOS, 20% PEG 3350, and 0.1 M cyclohexanone. This drop was suspended over a 1 mL reservoir in a 24-well ComboPlate (Greiner Bio-One), and the plate was incubated at 4 °C. Crystals suitable for diffraction studies grew in about one week.

Data were collected under standard cryogenic conditions on a Rigaku MicroMax-007HF generator equipped with VariMax HF optics and a Saturn 944+ CCD detector. The data were processed using the HKL2000 suite of programs (Table 1).[18] The structure was subsequently solved using Phaser,[19] employing $CHMO_{Open}$ (PDB ID 3GWF) as the search model.[11] The model was subjected to multiple rounds of positional and B-factor refinement using Refmac.[20] Manual model building was performed regularly during refinement using Coot.[21] The coordinates and structure factors have been deposited in the Protein Data Bank as PDB ID 3UCL. Structural figures were prepared using PyMOL (Schrödinger LLC).

Table 1. Data Collection and Refinement Statistics for the $CHMO_{Rotated}$ Crystal Structure (PDB ID 3UCL)

Data collection statistics	
Space group	$P2_12_12_1$
a, *b*, *c* (Å)	55.5, 67.1, 131.4
Resolution range (Å)[a]	30.6–2.4 (2.5–2.4)
Completeness (%)[a]	97.9 (92.7)
Redundancy[a]	11.2 (8.3)
R_{sym}[a]	8.7 (47.2)
Refinement statistics	
Total number of reflections (reflections in R_{free} set)	20,214 (2061)
R_{factor} (%) (Work + Free/Free)	19.8/26.4
Number of atoms	4215
Protein	3986
Water	121
Cofactors and Substrate	108
rmsd	
Bond length (Å)	0.017
Bond angle (deg)	1.669
Ramachandran plot	505 (100%)
Residues in favored positions	492 (97.4%)
Residues in allowed positions	10 (2.0%)
Residues in disallowed positions	3 (0.6%)

[a]Numbers in parentheses refer to the highest resolution shell.

Saturation Transfer Difference NMR Spectroscopy. The buffer used for dialysis of the protein was used to dissolve $NADP^+$ at 5 mM. Samples of the buffer and $NADP^+$ solution were placed under vacuum until dry, and then reconstituted in an equal volume of D_2O. A 600 μL sample of 75 μM protein and 1.5 mM $NADP^+$ was prepared. Samples of the protein without its ligand were also prepared as a control to confirm that all of the STD signals were derived from protein–ligand interactions.

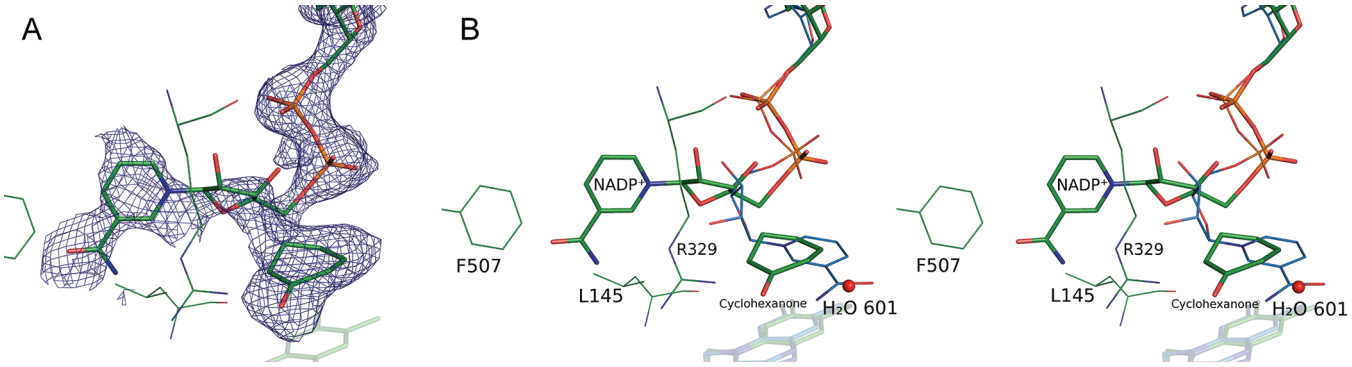

Figure 1. View of the active site in the $CHMO_{Rotated}$ (green) structure. The positions of FAD, $NADP^+$, and cyclohexanone are shown. (A) The $F_o - F_c$ electron density map contoured at 3.0σ around $NADP^+$ and cyclohexanone is shown as a blue mesh. The map was calculated with the ligands omitted from the model. (B) Stereo view with the position of $NADP^+$ in $CHMO_{Closed}$ (blue) overlaid on the $CHMO_{Rotated}$ crystal structure. Key residues R329, L145, and F507 and water molecule 601 are also shown.

All NMR experiments were performed at 15 °C on a Varian INOVA 500 MHz spectrometer equipped with a triple resonance HCN cold probe. A 1D saturation transfer difference pulse sequence with internal subtraction via phase cycling was employed to record difference spectra.[22] Residual HDO signal was removed using a double pulsed-field gradient spin echo. On-resonance irradiation of the protein was performed at −0.5 ppm, with off-resonance irradiation at 36.5 ppm. Reference spectra were recorded using the same pulse sequence with saturation pulses applied at 36.5 ppm, and no internal subtraction. Additional details regarding the NMR experiments are provided in the Supporting Information.

Enzyme Kinetics. All enzyme assays were performed at 22 °C using a Cary 50 Bio UV−Visible Spectrophotometer equipped with a Peltier-thermostatted cell. The enzyme, NADPH, and cyclohexanone were dissolved at the appropriate concentration in 50 mM sodium phosphate, pH 8.0. A 500 μL reaction volume was used. To determine the K_M and k_{cat} for NADPH, a series of assays with 100 μM cyclohexanone (>40× $K_{M(cyclohexanone)}$) and between 3 μM and 200 μM of NADPH were used. These experiments were repeated with varying concentrations of $NADP^+$ to determine the K_i of $NADP^+$. To determine the K_M and k_{cat} for cyclohexanone, a series of assays with 50 μM NADPH (>8× $K_{M(NADPH)}$) and between 0.4 μM and 40 μM cyclohexanone were used. A higher concentration of NADPH could not be used due to substrate inhibition. In all cases, the NADPH, 10 μL of an appropriate concentration of enzyme, and the substrate were mixed together to start the reaction. The decrease in absorbance at 340 nm was monitored to determine the initial rate of the oxidation reaction. The initial rates were plotted against the substrate (NADPH or cyclohexanone) concentration for each reaction series, and nonlinear regression was performed using SigmaPlot (Systat Software, Inc.) to determine the K_M and k_{cat}.

A second set of experiments were performed to determine the uncoupling ratio, defined as the rate of NADPH oxidation in the presence of cyclohexanone (apparent BV activity) divided by the rate of NADPH oxidation in the absence of cyclohexanone (NADPH oxidase activity). Using saturating concentrations of both NADPH (>6× $K_{M(NADPH)}$) and cyclohexanone (>40× $K_{M(cyclohexanone)}$), the decrease in absorbance at 340 nm was assessed both before and after the addition of cyclohexanone. Three different NADPH concentrations were used (40−80 μM), all of which saturated the enzyme, and the experiments were conducted in quadruplets.

RESULTS

Crystal Structure of Substrate-Bound CHMO. The crystal structure of *Rm*CHMO in complex with FAD, $NADP^+$, and cyclohexanone was obtained to a resolution of 2.4 Å (Table 1). The polypeptide backbone could be modeled completely from residues 5−534, with the exception of two unstructured loop regions from residues 146−149 and 489−503. The first loop region corresponds to a long linker between the FAD- and NADPH-binding domains, while the second corresponds to the large loop that is unstructured in the $CHMO_{Open}$ structure, but folds in to contact $NADP^+$ in the $CHMO_{Closed}$ structure. Density consistent with FAD, $NADP^+$, and cyclohexanone was also visible (Figure 1A). To differentiate it from the $CHMO_{Open}$ and $CHMO_{Closed}$ structures that were previously reported, we will refer to this structure as $CHMO_{Rotated}$.

In general, the $CHMO_{Rotated}$ structure most closely resembles the $CHMO_{Open}$ structure (rmsd of 0.56 Å between backbone atoms present in both $CHMO_{Open}$ and $CHMO_{Rotated}$ structures when the FAD-binding domains are aligned, vs 1.31 Å for $CHMO_{Closed}$). When aligning the two structures based on their FAD-binding domains, the FAD-binding and helical domains show very little structural divergence. The NADPH-binding domain shows a slight rotation, though this is significantly less pronounced than the substantial domain movements seen when comparing the $CHMO_{Open}$ and $CHMO_{Closed}$ structures. This rotation allows for a subtle shift in the position of the adenine portion of $NADP^+$, which may in turn trigger the rotation of its nicotinamide moiety.

Rotation of the $NADP^+$ Cofactor. One of the most significant features in the crystal structure is the large rotation of the nicotinamide phosphoribose of $NADP^+$ when compared to $CHMO_{Open}$ and $CHMO_{Closed}$ (Figure 1B). It is for this reason that we refer to it as the $CHMO_{Rotated}$ structure. This rotation serves to displace the nicotinamide head away from its position above the isoalloxazine ring system of FAD and into the large, primarily hydrophobic cavity that is seen in the $CHMO_{Open}$ structure. This movement has two notable effects. By rotating away from the FAD ring system, space for the substrate to enter into the catalytic position is created. Second, the nicotinamide head serves to partially block the active site region from the bulk solvent, which prevents the substrate from diffusing back into solution while the protein is in the Rotated conformation (Figure 2). It is notable that the nicotinamide moiety forms relatively few strong interactions in this conformation.

The new conformation of $NADP^+$ allows the formation of intramolecular hydrogen bonds between the 3′ hydroxyl of the nicotinamide ribose and both the nicotinamide and the adenine phosphates. This intramolecular interaction stabilizes this conformation of the $NADP^+$ and may be a driving force in the adoption of this conformation.

dx.doi.org/10.1021/ja211876p | J. Am. Chem. Soc. 2012, 134, 7788−7795

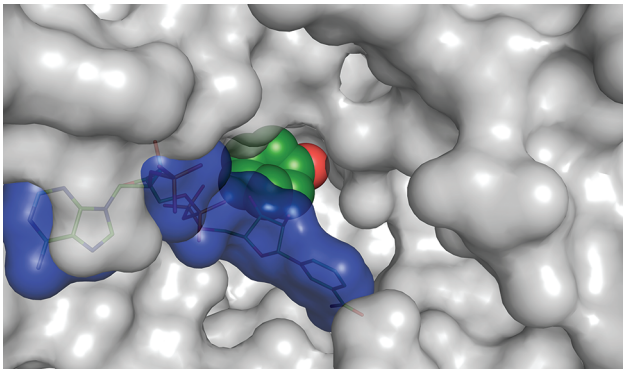

Figure 2. $NADP^+$ blocks cyclohexanone from diffusing into the bulk solvent in the Rotated conformation. The protein surface is shown in gray. $NADP^+$ is shown in stick representation and its surface is outlined in blue. Cyclohexanone is shown using green space-filling representation.

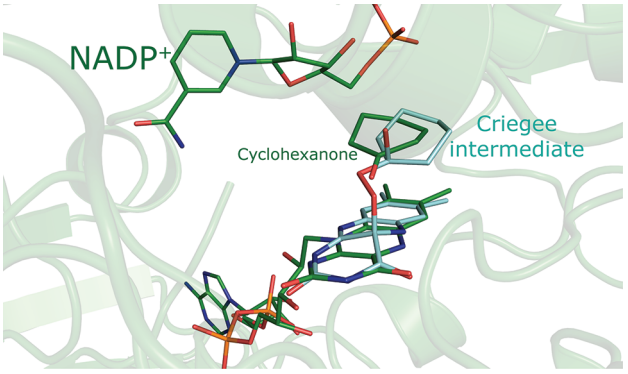

Figure 3. The $CHMO_{Rotated}$ crystal structure (green) is shown superimposed on a model of the Criegee intermediate (cyan). The model was produced using molecular dynamics followed by energy minimization in Chem3D, while enforcing the antiperiplanar geometry required for migration of the carbon.

The Binding of the Substrate, Cyclohexanone. Electron density corresponding in size and shape to what is expected for cyclohexanone was observed above the isoalloxazine ring system of FAD; therefore, we proceeded to model the substrate at this position (Figure 1A). The carbonyl oxygen of cyclohexanone appears to be oriented through interactions with D59 and R329. Both of these residues have been previously implicated in controlling the position of $NADP^+$,[11,13,23] as well as in the positioning of a weak inhibitor of PAMO.[14] A nearby water molecule (H_2O 601) also forms a weak hydrogen bond with the carbonyl oxygen, linking it to Q192, the backbone atoms of residues L57 and D59, and a larger solvent network.

It is known that the formation of the Criegee intermediate, the key catalytic step in the BVMO reaction mechanism, involves a nucleophilic attack on the carbonyl carbon of cyclohexanone by the peroxyanion intermediate, in which the peroxyanion is covalently linked to the C4X carbon of FAD. The distance between C4X and the carbonyl carbon is 3.9 Å in this crystal structure. With the FAD-linked oxygen of the peroxide group expected to occupy an axial position relative to the FAD ring system, if the anionic oxygen were to point toward cyclohexanone, the position occupied by cyclohexanone in this structure would correspond approximately to the expected position for the nucleophilic attack and formation of the Criegee intermediate. A model of the Criegee intermediate that imposes antiperiplanar geometry required for migration of the carbon to form the lactone[24] shows that cyclohexanone nearly coincides with its position in the model of the intermediate (Figure 3). A shift of ~0.5 Å is required to superimpose the carbonyl carbon of the cyclohexanone molecule and the intermediate, after which a ~30° rotation is sufficient to make the molecules overlap.

Structure–Function Studies Probing the Rotated Conformation. To probe the relevance of the observed Rotated conformation for catalysis, we designed three mutants that were predicted to specifically perturb nicotinamide cofactor binding in the Rotated conformation, while having no impact on the cofactor in either the Open or Closed conformations. The three mutants, L145N, L145D, and F507Y, are anticipated to stabilize the catalytic conformation by forming a polar contact with the carboxamide group of $NADP^+$ in the Rotated conformation. In contrast, in the $CHMO_{Open}$ and $CHMO_{Closed}$ structures, these residues should not interact directly with the cofactor, with the nearest distance in either structure being more than 5 Å. Given that many of the residues implicated in $NADP^+$-binding in the $CHMO_{Rotated}$ structure are also involved in substrate specificity, the rational design of destabilizing mutations specific for the Rotated conformation was not feasible.

To assess the degree of perturbation in the $NADP^+$ binding mode caused by these mutations, transferred nuclear Overhauser effect (Tr-NOE) and saturation transfer difference (STD) NMR experiments were performed. No major differences were observed between the Tr-NOESY spectra of $NADP^+$ in the presence of wild-type CHMO or any of the three mutants, as only some slight changes of NOE intensities and appearance and disappearance of the weakest NOEs were observed. This suggests that the overall set of conformations available to $NADP^+$ in the mutants is not significantly perturbed. In the STD experiments, the aim was to assess if there was a difference in the relative enhancement of the STD effect of the pyridine protons as compared to the adenine protons when the mutants were compared to the wild-type protein. The differences observed were subtle, and preclude a discussion of the effects of the mutations on any individual proton; however, when the STD effect of the four protons on the pyridine ring (N2, N4, N5, and N6) was compared to the STD effect for the two adenine ring protons (A2 and A8, where A2 is used as the reference for the STD effect), a trend could be observed (Supporting Information Figure S1). The interactions between the protein and the pyridine protons appeared closer than the protein–adenine proton interactions in the mutants as compared to the wild-type CHMO. This is consistent with a minor selective stabilization of the nicotinamide moiety binding mode in the Rotated conformation.

While the structural impact of the mutants was subtle, as assessed by NMR methods, the impact on the kinetic properties of CHMO was substantial (Figure 4, see Supporting Information Table S1 for complete kinetic data). In comparing the K_M values for NADPH, the wild-type had the highest K_M, suggesting that all three mutants bind the cofactor more strongly during catalysis. It should be noted that all the K_M values were within an order of magnitude of each other. Furthermore, in terms of k_{cat}, all three mutants had substantially lower rates than the wild-type, with the k_{cat} dropping by at least a factor of 6 and by as much as a factor of 100. This effect was seen for the k_{cat} of both NADPH and cyclohexanone. This

dx.doi.org/10.1021/ja211876p | J. Am. Chem. Soc. 2012, 134, 7788–7795

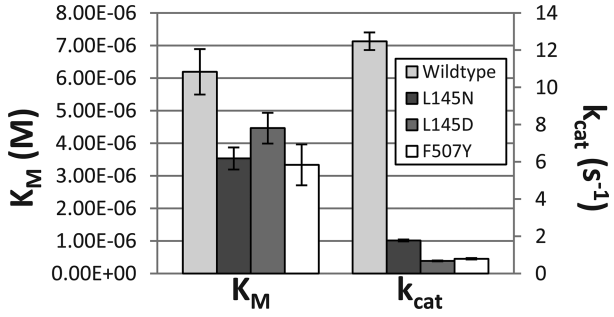

Figure 4. The K_M and k_{cat} of NADPH for the wild-type and the three mutants are shown. Error bars correspond to the standard error as determined by nonlinear regression.

shows that, although the binding affinity of NADPH had been slightly improved, the mutations appear to have significantly slowed the reaction rate. The K_i for $NADP^+$ as a competitive inhibitor of CHMO is discussed in the Supporting Information, and is largely consistent with the observed trend for $NADP^+$ binding affinities in the mutants.

The uncoupling ratio is an indicator of the efficiency of the complete Baeyer–Villiger reaction (BV activity) relative to the efficiency at which NADPH would be used in the absence of cyclohexanone (NADPH oxidase activity). The wild-type enzyme exhibits the largest uncoupling ratio of 114. For the three mutants, this ratio is significantly reduced, ranging from 4 to 20. To assess how much of this change is caused by the decrease in BV activity and how much is due to changes in the amount of unproductive NADPH oxidase activity, the normalized uncoupling ratio was compared to the normalized $k_{cat}/K_{M(NADPH)}$ and $k_{cat}/K_{M(cyclohexanone)}$ values, using the wild-type values as 100% (Supporting Information Figure S2). Note that both k_{cat}/K_M values were determined using the apparent BV activity (which includes unproductive NADPH oxidase activity in the presence of cyclohexanone), not the uncoupled reaction (NADPH oxidase activity). For all three mutants, the uncoupling ratio was significantly greater than would be predicted by the normalized $k_{cat}/K_{M(cyclohexanone)}$, and moderately smaller than predicted by the normalized $k_{cat}/K_{M(NADPH)}$.

DISCUSSION

A Third $NADP^+$ Conformation. Previous structural studies of BVMOs have raised a critical question: how is the enzyme capable of effecting catalysis with a structure that has its active site blocked by the $NADP^+$ cofactor? The $NADP^+$ has been shown to be bound throughout the catalytic cycle,[23,25,26] presumably to stabilize the peroxyanion intermediate, precluding the possibility of dissociation of $NADP^+$ prior to substrate binding. At the same time, much of the space required for the substrate to form the expected Criegee intermediate is blocked by $NADP^+$ and other key residues. The rotation of the nicotinamide away from the FAD provides an explanation for how the substrate can enter the space close to the peroxyanion intermediate while $NADP^+$ remains bound. In this conformation, the substrate sits in a putative catalytic position that is large enough to accommodate CHMO's larger substrates. While the structure resembles the Open conformation, the rotation of the $NADP^+$ nicotinamide blocks off much of the space that is available in the $CHMO_{Open}$ structure (Figure 2), and a shifting of the key residue, R329, narrows the channel further to prevent the substrate from diffusing away from the peroxyanion intermediate. In this way, the substrate is "locked" into the active site pocket in the Rotated conformation. We propose that in order to avoid the rapid collapse of the peroxyanion intermediate, the substrate is bound in the previously reported Open and Closed conformations. The relatively weak interactions between the nicotinamide and the protein in the Rotated conformation would disfavor this conformation unless the substrate was able to replace some of the lost interactions. In other words, the enzyme would be locked in a conformation that stabilizes the peroxyanion intermediate until the substrate is present in the substrate binding site observed in the $CHMO_{Closed}$ structure. At that point, the enzyme can switch into the Rotated conformation, allowing catalysis to occur.

The NMR and kinetic data for wild-type and CHMO mutants are in agreement with this proposal. The three mutants were designed such that the altered residues would form favorable interactions specifically with the observed Rotated conformation of the nicotinamide cofactor while having no interactions with this cofactor in either the Open or Closed conformations of the enzyme. The NMR data supports that the design of the mutants was successful as the STD data for the mutants show that the pyridine moiety is bound with higher affinity relative to the adenine moiety. This is consistent with the stabilization of a minor conformational state for the pyridine moiety akin to that observed in the $CHMO_{Rotated}$ structure. Kinetic studies reveal that the mutants display a moderate increase in the affinity of $NADP^+$, as seen by the decrease in K_M. This observation strongly suggests that the Rotated conformation is an enzyme state that must occur sometime during the reaction cycle of CHMO. Moreover, the reaction rate is significantly decreased (6- to 100-fold). This change in k_{cat} for the mutants implies that the enzyme is spending longer than usual in one or perhaps more catalytically critical steps during the reaction cycle. Finally, the uncoupling ratio data provide insight into which specific step in the reaction mechanism might be delayed. For reasons discussed in the Supporting Information, the uncoupling data are consistent with the interpretation that the mutants are less efficient in stabilizing the peroxyanion intermediate, compared to the wild-type enzyme. This is in agreement with the adoption of the Rotated conformation prior to the binding of the ketone substrate in the mutants, leading to the destabilization of the peroxyanion intermediate and uncoupling of NADPH consumption from BV activity. Given that this is the case, it would be expected that the Rotated conformation most likely occurs when the ketone substrate is present, as we propose based on our structural data.

The Rotated structure highlights the need of this enzyme to adopt several arrangements of the substrates and cofactors in order to catalyze the elaborate chemical mechanism. This is a phenomenon seen in other flavoenzymes, including the well-studied *para*-hydroxybenzoate hydroxylase[27–31] and phenol hydroxylase,[32,33] the former being one of the first flavoenzymes to have its structure solved. Like the BVMOs, these hydroxylases face the problem of needing to bring the substrate in close proximity to a flavin peroxide intermediate that is inherently unstable in protic solvents.[34] The details and order of substrate and cofactor binding and release are different, as are the solutions employed to overcome this problem. In spite of this, both the hydroxylases and the BVMOs employ changes in the relative arrangements of the substrates and cofactors at different stages of their catalytic mechanisms to protect the peroxide while permitting the reaction of the substrate to

dx.doi.org/10.1021/ja211876p | J. Am. Chem. Soc. 2012, 134, 7788–7795

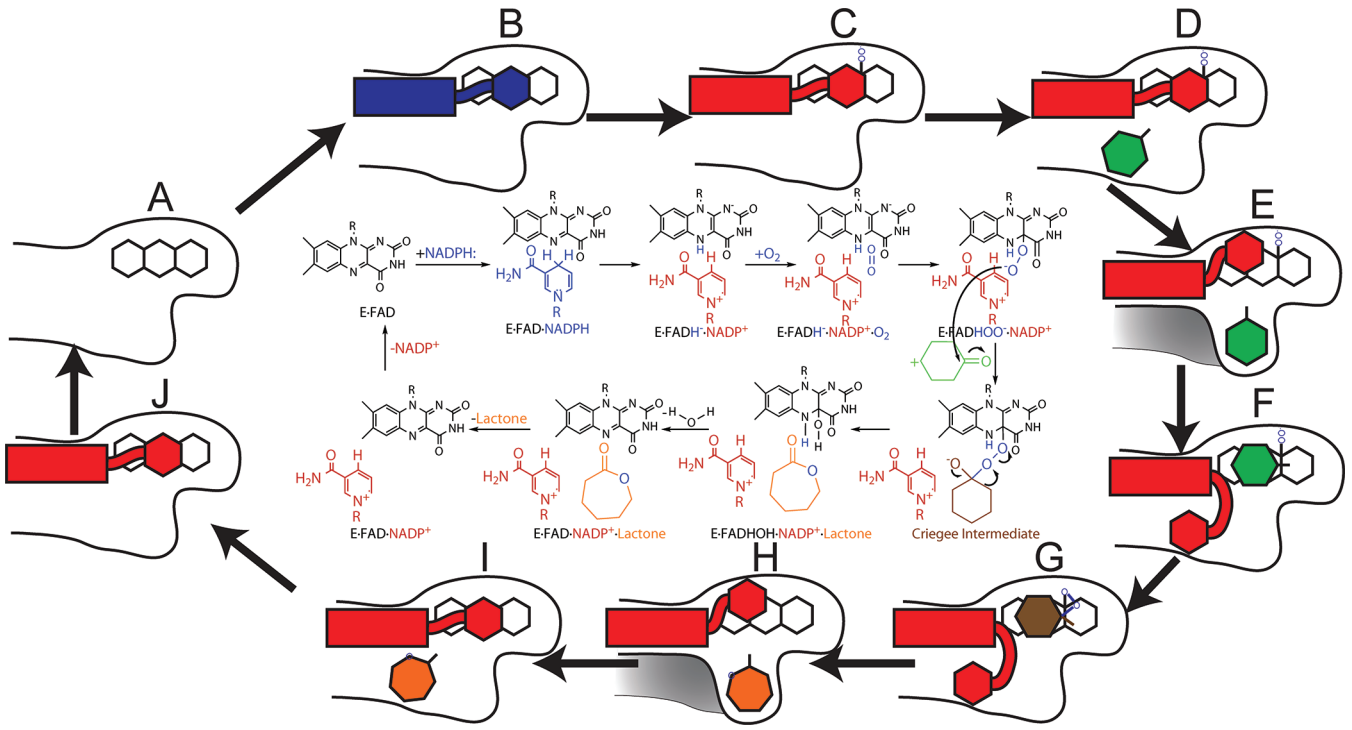

Figure 5. Schematic of the proposed mechanism for CHMO. The schematics are labeled A to J to correspond to the states referred to in the text. Both the schematics and the chemical mechanism shown in the center are colored using the same scheme. The FAD is denoted by three fused hexagons. The reduced NADPH is shown in blue, with the adenine portion as a rectangle, the nicotinamide as a hexagon, and the phosphate backbone as a thick wavy line. The oxidized $NADP^+$ is shown in red. The substrate is shown in green, the lactone in orange, and the Criegee intermediate in brown. The peroxyanion moiety is shown in blue attached to the FAD.

occur.[34] The hydroxylases employ three conformations, involving a large rotation of the FAD cofactor, to move from a substrate binding position[31] to a flavin reduction position[27,28] and finally to a substrate hydroxylation position.[27,29,30] With CHMO, it is the $NADP^+$ that moves from a flavin reduction position to a substrate binding position and finally to the Criegee position. In both cases, the peroxyanion intermediate is maintained in a protected environment until the moment that the reaction with the substrate can occur.[34]

This does not mark the first time a flavin-dependent monooxygenase (FMO) has been observed to have $NADP^+$ present in a rotated conformation. In a recent study, two crystal structures of an FMO from *Methylophaga* sp. strain SK1 (*m*FMO) were obtained with a similar conformation of $NADP^+$ (Supporting Information Figure S3).[35] These structures were obtained using a mutant enzyme or a $NADP^+$ analogue. As *m*FMO has substantial structural differences as compared to CHMO, the minor differences in the conformation are to be expected. As *m*FMO has a much more open structure than CHMO, there is no need for the enzyme to adopt an alternate conformation to allow catalysis to occur. As such, this conformation is considered to be a product of the high promiscuity of *m*FMO.[35] With CHMO, we can see this as being a critical conformation during the catalytic cycle.

The Catalytic Position of Cyclohexanone. The $CHMO_{Rotated}$ structure unveils the position of CHMO immediately prior to the reaction with the peroxyanion intermediate to form the Criegee intermediate. Indeed, we see the substrate close to the ideal geometry for catalysis to occur. Assuming that the peroxyanion intermediate were to form prior to adoption of this conformation, a slight shift in the position of the substrate would result in the necessary geometry for nucleophilic attack on the carbonyl carbon of the ketone. In addition, a fairly minor rotation will result in the antiperiplanar geometry required for the migrating group to form the necessary bond with the peroxide oxygen.

Intriguingly, many of the residues previously implicated in determining the substrate specificity of CHMO and other BVMOs,[36−43] which generally line the pocket observed in the $CHMO_{Closed}$ structure, are not in the vicinity of the substrate in the $CHMO_{Rotated}$ structure. This suggests that the Rotated conformation is not the most important conformation for determining substrate specificity, regiospecificity, and enantiospecificity of the enzyme. Rather, the putative substrate binding pocket observed in the $CHMO_{Closed}$ structure is critical in determining the substrate profile of the enzyme. We can speculate that the key residue R329 may play a role in guiding the substrate from the Closed conformation pocket to the Rotated conformation position while maintaining the chemo-, regio-, and enantiospecificity dictated by the $CHMO_{Closed}$ structure.

Given the apparent necessity for a substrate-bound form in the Closed conformation, it appears likely that CHMO employs a series of conformational changes to gradually move the substrate from the solvent into the position observed in the $CHMO_{Rotated}$ structure. In contrast to this, a recent study has reported multiple structures of PAMO with bound $NADP^+$,[14] all of which were obtained in a conformation similar to the $CHMO_{Closed}$ structure, and some of which also had bound MES, a weak inhibitor of PAMO. The MES inhibitor was observed in a funnel-shaped cavity leading to the catalytic site, suggesting that this is a potential route for the substrate to enter the active site. This arrangement has been previously observed in other flavoproteins, like ornithine hydroxylase.[44] In CHMO,

dx.doi.org/10.1021/ja211876p | *J. Am. Chem. Soc.* 2012, 134, 7788−7795

this funnel is blocked by a dipeptide insert that is missing in PAMO (residues 278−279, CHMO numbering) (Supporting Information Figure S4), precluding its use for substrate binding in *Rm*CHMO. On the basis of sequence alignments, this dipeptide insert is conserved in almost all CHMOs, including *Ac*CHMO, as well as a number of other closely related BVMOs. The funnel is also blocked in the structures of OTEMO.[15] It might be that BVMOs like CHMO and OTEMO use different mechanisms for substrate binding as compared to PAMO: the former by adopting a series of conformations that progressively move the substrate toward the catalytic position, and the latter via a tunnel that allows for a "back door" access. The possibility that CHMO and PAMO employ slightly different mechanisms is not new; when the detailed kinetic mechanism for PAMO was elucidated,[23] it was seen that a spectral change associated with a conformational change during $NADP^+$ release in CHMO[26] was not observed. It is also possible that the more limited substrate profile of PAMO as compared to other BVMOs[37,40,42,45] is related to this differing substrate binding mechanisms.

A Structural Mechanism for BVMO Catalysis. The $CHMO_{Rotated}$ structure allows us to propose a mechanism for BVMO catalysis from a structural perspective that is consistent with the previously elucidated kinetic mechanism of BVMOs.[23,25,26] The structural states referred to here will correspond to the states shown in Figure 5. The catalytic mechanism begins in the NADP(H)- and substrate-free form (*state A*). Following binding of NADPH (*state B*) and reduction of FAD in an Open-like conformation, the $NADP^+$, R329, and D59 will occupy positions that stabilize the reduced flavin. Molecular oxygen will react with the reduced flavin, forming the peroxyanion intermediate (*state C*), which is also stabilized by the same residues. This would also likely take place in a state resembling the Open conformation. The substrate will then bind weakly in the diffuse binding pocket observed in the $CHMO_{Open}$ structure (*state D*). This will trigger the reorganization of the large, unstructured loop, permitting the enzyme to adopt a tight-binding, $CHMO_{Closed}$-like structure (*state E*). It is this structure that will determine whether a substrate will be accepted by the enzyme, as well as what the regio- and enantiospecificity will be. From there, the enzyme will switch into the peroxyanion intermediate version of the Rotated conformation. This involves the rotation of $NADP^+$, the migration of the substrate into the catalytic position, and the shifting of R329 (*state F*). We speculate that R329 plays the role of a chaperone guiding the substrate into the catalytic position without allowing it to reorient. This would allow the preservation of the stereochemical requirements imposed in the Closed conformation. At the same time, $NADP^+$ obstructs the exit pathway, preventing the substrate from diffusing away from the reaction site. Formation of the Criegee intermediate will occur (*state G*), followed by the formation of the lactone product. Once the product is formed, the enzyme will reverse its steps. The R329 will reposition the product, allowing the $NADP^+$ to return to its position above the flavin rings. This may occur in two stages, with the lactone returning to the tight-binding pocket in the $CHMO_{Closed}$ structure (*state H*) before switching to the Open conformation (*state I*), or it may switch to the Open conformation directly (*state I*). Either way, the Open conformation causes the product to be bound again in the loose-binding mode. The product can then be released to the solvent (*state J*), followed by the release of the oxidized $NADP^+$ cofactor, and the return of the enzyme to the initial state (*state A*).

The schematic shown in Figure 5 emphasizes the fact that the protein accommodates a variety of ligand positions, of which three have been observed directly with crystal structures. In spite of this, it appears to do so using only two major global protein conformations: Open-like conformations and Closed-like conformations.

CONCLUSION

Up to now, there has been a considerable gap in our understanding of the structural mechanism of the BVMOs. The lack of a crystal structure with the substrate bound to the enzyme has prevented a structural description of the enzyme state allowing for the formation of the Criegee intermediate. The structure presented here shows for the first time a catalytically competent structure of a BVMO. Indeed, it places the ketone substrate in an ideal position for the formation of the Criegee intermediate. At the same time, it provides the necessary space and flexibility for the accommodation of a wide range of substrates of various sizes. Finally, it provides a solution to the problem of how the substrate can reach the active site while the $NADP^+$ cofactor remains bound that is consistent with the established kinetic mechanism. This fills a critical gap in understanding of the catalytic mechanism of the BVMOs, and has allowed us to propose a structural description of the mechanism of this family of enzymes.

ASSOCIATED CONTENT

Supporting Information

Subcloning of the *chnB1* gene; creation of the L145N, L145D, and F507Y mutants; expression and purification of CHMO; detailed STD procedure; STD results; uncoupling ratio results; comparison of $CHMO_{Rotated}$ to *m*FMO structures; comparison of the "back" of CHMO and PAMO; complete kinetics data; $NADP^+$ inhibition results; and discussion of the uncoupling ratio results. This material is available free of charge via the Internet at http://pubs.acs.org.

AUTHOR INFORMATION

Corresponding Author

albert.berghuis@mcgill.ca

Notes

The authors declare no competing financial interest.

ACKNOWLEDGMENTS

The authors thank past and present members of the Berghuis and Lau laboratories for their assistance and suggestions. We would like to thank Roderick MacCuish in particular for his help in creating the CHMO mutants and preparing protein for NMR. We would also like to thank Joelle Pelletier for helpful discussions regarding the enzyme kinetics. The research was made possible through grants from the Natural Sciences and Engineering Research Council of Canada and Canadian Institute of Health Research awarded to A.M.B. B.J.Y. has held scholarships from the Natural Sciences and Engineering Research Council of Canada, McGill University, and the CIHR Strategic Initiative in Chemical Biology. A.M.B. holds a Canada Research Chair in Structural Biology. NMR experiments were performed at the Québec/Eastern Canada High Field NMR Facility, which is supported by grants from the Natural Sciences

and Engineering Research Council of Canada and the Québec ministère de la recherche en science et technologie.

REFERENCES

(1) Baeyer, A.; Villiger, V. *Ber. Dtsch. Chem. Ges.* **1899**, *32*, 3625−3633.
(2) Baeyer, A.; Villiger, V. *Ber. Dtsch. Chem. Ges.* **1900**, *33*, 858−864.
(3) ten Brink, G. J.; Arends, I. W. C. E.; Sheldon, R. A. *Chem. Rev.* **2004**, *104*, 4105−4124.
(4) de Gonzalo, G.; Mihovilovic, M. D.; Fraaije, M. W. *ChemBioChem* **2010**, *11*, 2208−2231.
(5) Alphand, V.; Wohlgemuth, R. *Curr. Org. Chem.* **2010**, *14*, 1928−1965.
(6) Leisch, H.; Morley, K.; Lau, P. C. K. *Chem. Rev.* **2011**, *111*, 4165−4222.
(7) Lau, P. C. K.; Leisch, H.; Yachnin, B. J.; Mirza, I. A.; Berghuis, A. M.; Iwaki, H.; Hasegawa, Y. In *Green Polymer Chemistry: Biocatalysis and Biomaterials*; Cheng, H. N., Gross, R. A., Eds.; American Chemical Society: Washington, DC, 2010; Vol. *1043*, pp 343−372.
(8) Kayser, M. M. *Tetrahedron* **2009**, *65*, 947−974.
(9) Torres Pazmiño, D. E.; Dudek, H. M.; Fraaije, M. W. *Curr. Opin. Chem. Biol.* **2010**, *14*, 138−144.
(10) Donoghue, N. A.; Trudgill, P. W. *Eur. J. Biochem.* **1975**, *60*, 1−7.
(11) Mirza, I. A.; Yachnin, B. J.; Wang, S.; Grosse, S.; Bergeron, H.; Imura, A.; Iwaki, H.; Hasegawa, Y.; Lau, P. C. K.; Berghuis, A. M. *J. Am. Chem. Soc.* **2009**, *131*, 8848−8854.
(12) Donoghue, N. A.; Norris, D. B.; Trudgill, P. W. *Eur. J. Biochem.* **1976**, *63*, 175−192.
(13) Malito, E.; Alfieri, A.; Fraaije, M. W.; Mattevi, A. *Proc. Natl. Acad. Sci. U.S.A.* **2004**, *101*, 13157−13162.
(14) Orru, R.; Dudek, H. M.; Martinoli, C.; Torres Pazmiño, D. E.; Royant, A.; Weik, M.; Fraaije, M. W.; Mattevi, A. *J. Biol. Chem.* **2011**, *286*, 29284−29291.
(15) Leisch, H.; Shi, R.; Grosse, S.; Morley, K.; Bergeron, H.; Cygler, M.; Iwaki, H.; Hasegawa, Y.; Lau, P. C. K. *Appl. Environ. Microbiol.* **2012**, *78*, 2200−2212.
(16) Beam, M. P.; Bosserman, M. A.; Noinaj, N.; Wehenkel, M.; Rohr, J. *Biochemistry* **2009**, *48*, 4476−4487.
(17) Polyak, I.; Reetz, M. T.; Thiel, W. *J. Am. Chem. Soc.* **2012**, *134*, 2732−2741.
(18) Otwinowski, Z.; Minor, W. In *Methods in Enzymology*; Academic Press: 1997; Vol. *276*, pp 307−326.
(19) McCoy, A. J.; Grosse-Kunstleve, R. W.; Adams, P. D.; Winn, M. D.; Storoni, L. C.; Read, R. J. *J. Appl. Crystallogr.* **2007**, *40*, 658−674.
(20) Murshudov, G. N.; Vagin, A. A.; Dodson, E. J. *Acta Crystallogr., Sect. D: Biol. Crystallogr.* **1997**, *D53*, 240−255.
(21) Emsley, P.; Cowtan, K. *Acta Crystallogr., Sect. D: Biol. Crystallogr.* **2004**, *D60*, 2126−2132.
(22) Mayer, M.; Meyer, B. *J. Am. Chem. Soc.* **2001**, *123*, 6108−6117.
(23) Torres Pazmiño, D. E.; Baas, B.-J.; Janssen, D. B.; Fraaije, M. W. *Biochemistry* **2008**, *47*, 4082−4093.
(24) Snowden, M.; Bermudez, A.; Kelly, D. R.; Radkiewicz-Poutsma, J. L. *J. Org. Chem.* **2004**, *69*, 7148−7156.
(25) Ryerson, C. C.; Ballou, D. P.; Walsh, C. T. *Biochemistry* **1982**, *21*, 2644−2655.
(26) Sheng, D.; Ballou, D. P.; Massey, V. *Biochemistry* **2001**, *40*, 11156−11167.
(27) Gatti, D. L.; Palfey, B. A.; Lah, M. S.; Entsch, B.; Massey, V.; Ballou, D. P.; Ludwig, M. L. *Science* **1994**, *266*, 110−114.
(28) Schreuder, H. A.; Mattevi, A.; Obmolova, G.; Kalk, K. H.; Hol, W. G. J.; van der Bolt, F. J. T.; van Berkel, W. J. H. *Biochemistry* **1994**, *33*, 10161−10170.
(29) Schreuder, H. A.; Prick, P. A. J.; Wierenga, R. K.; Vriend, G.; Wilson, K. S.; Hol, W. G. J.; Drenth, J. *J. Mol. Biol.* **1989**, *208*, 679−696.
(30) Schreuder, H. A.; van der Laan, J. M.; Hol, W. G. J.; Drenth, J. *J. Mol. Biol.* **1988**, *199*, 637−648.
(31) Wang, J.; Ortiz-Maldonado, M.; Entsch, B.; Massey, V.; Ballou, D. P.; Gatti, D. L. *Proc. Natl. Acad. Sci. U.S.A.* **2002**, *99*, 608−613.
(32) Enroth, C.; Neujahr, H.; Schneider, G.; Lindqvist, Y. *Structure* **1998**, *6*, 605−617.
(33) Xu, D.; Ballou, D. P.; Massey, V. *Biochemistry* **2001**, *40*, 12369−12378.
(34) Entsch, B.; Cole, L. J.; Ballou, D. P. *Arch. Biochem. Biophys.* **2005**, *433*, 297−311.
(35) Orru, R.; Pazmiño, D. E. T.; Fraaije, M. W.; Mattevi, A. *J. Biol. Chem.* **2010**, *285*, 35021−35028.
(36) Reetz, M. T.; Brunner, B.; Schneider, T.; Schulz, F.; Clouthier, C. M.; Kayser, M. M. *Angew. Chem., Int. Ed.* **2004**, *43*, 4075−4078.
(37) Bocola, M.; Schulz, F.; Leca, F.; Vogel, A.; Fraaije, M. W.; Reetz, M. T. *Adv. Synth. Catal.* **2005**, *347*, 979−986.
(38) Mihovilovic, M. D.; Rudroff, F.; Winninger, A.; Schneider, T.; Schulz, F.; Reetz, M. T. *Org. Lett.* **2006**, *8*, 1221−1224.
(39) Kayser, M. M.; Clouthier, C. M. *J. Org. Chem.* **2006**, *71*, 8424−8430.
(40) Torres Pazmiño, D. E.; Snajdrova, R.; Rial, D. V.; Mihovilovic, M. D.; Fraaije, M. W. *Adv. Synth. Catal.* **2007**, *349*, 1361−1368.
(41) Reetz, M. T.; Wu, S. *Chem. Commun. (Cambridge, U.K.)* **2008**, 5499−5501.
(42) Reetz, M. T.; Wu, S. *J. Am. Chem. Soc.* **2009**, *131*, 15424−15432.
(43) Dudek, H. M.; de Gonzalo, G.; Torres Pazmiño, D. E.; Stepniak, P.; Wyrwicz, L. S.; Rychlewski, L.; Fraaije, M. W. *Appl. Environ. Microbiol.* **2011**, *77*, 5730−5738.
(44) Olucha, J.; Meneely, K. M.; Chilton, A. S.; Lamb, A. L. *J. Biol. Chem.* **2011**, *286*, 31789−31798.
(45) Fraaije, M. W.; Wu, J.; Heuts, D. P. H. M.; van Hellemond, E. W.; Spelberg, J. H. L.; Janssen, D. B. *Appl. Microbiol. Biotechnol.* **2005**, *66*, 393−400.